
DEFLAGRATION-TO-DETONATION TRANSITION IN AN UNCONFINED SPACE: II. EXPANDING HYDROGEN-OXYGEN FLAMES

A PREPRINT

Andrey Koksharov
School of Mathematical Sciences
Sackler Faculty of Exact Sciences
Tel Aviv University
Tel Aviv 69978
koksharov@gmx.net

Leonid Kagan
School of Mathematical Sciences
Sackler Faculty of Exact Sciences
Tel Aviv University
Tel Aviv 69978
kaganleo@tauex.tau.ac.il

Gregory Sivashinsky
School of Mathematical Sciences
Sackler Faculty of Exact Sciences
Tel Aviv University
Tel Aviv 69978
grishas@tauex.tau.ac.il

June 28, 2019

ABSTRACT

The problem of deflagration-to-detonation transition in an unconfined environment is revisited. With a freely expanding self-accelerating hydrogen-oxygen flame as an example, it is shown that deflagration-to-detonation transition is indeed possible provided the flame is large enough. The transition occurs prior to merging of the flame with the flame-supported precursor shock. The pre-transition flame does not reach the threshold of CJ-deflagration. Numerical simulations employed are based on the recently developed pseudo-spectral method with time and space adaptation.

Keywords Deflagration-to-detonation transition · Accelerating flames · Thermal runaway of fast flames · Computational reactive fluid dynamics

1 Introduction

In part 1 of this article [1] it is shown that a freely expanding self-accelerating spherical flame governed by a one-step Arrhenius kinetics coupled with Darrieus-Landau wrinkling undergoes an abrupt transition to detonation (DDT) when the flame radius R_f reaches a critical value, R_{ddt} . In the present paper to assess R_{ddt} for a realistic multistep chemistry and multicomponent transport we explore the case of a stoichiometric hydrogen-oxygen system, $2\text{H}_2 + \text{O}_2$, initially at $T_0 = 300\text{ K}$ and $P_0 = 1\text{ bar}$.

The results obtained substantiate qualitative predictions of [1], yielding $R_{ddt} = 10\text{ m}$ noticeably behind the precursor shock (s) for which $R_{s,ddt} = 11.5\text{ m}$.

2 Mathematical model

In spherical symmetry, the set of governing equations for state variables velocity in radial direction u , temperature T and concentrations of reactants c_i reads as

Momentum conservation

$$\frac{\partial}{\partial t} (r^2 \rho u) + \frac{\partial}{\partial r} \left(r^2 (\rho u^2 + \tau_{rr}) \right) = -r^2 \frac{\partial P}{\partial r} + r (\tau_{\theta\theta} + \tau_{\varphi\varphi}), \quad (1)$$

Energy conservation

$$\frac{\partial}{\partial t} (r^2 \rho e) + \frac{\partial}{\partial r} \left(r^2 \left(u (\rho e + P + \tau_{rr}) + \sum_{i=1}^{n_s} h_i j_i^d - \lambda \frac{\partial T}{\partial r} \right) \right) = 0, \quad (2)$$

Species conservation

$$\frac{\partial}{\partial t} (r^2 c_i) + \frac{\partial}{\partial r} \left(r^2 (uc_i + j_i^d) \right) = r^2 \Sigma^2 \dot{\omega}_i, \quad i = 1, \dots, n_s, \quad (3)$$

Here n_s – number of species, $\dot{\omega}_i$ – chemical source of species, j_i^d – molar diffusion flux, h_i – molar enthalpy, and Σ is the degree of folding [2] – the ratio of the total area of the wrinkled front to the area associated with its average radius R_f . The reason for Σ^2 in Eq. 3 is explained as follows. According to the classical Zel’dovich–Frank–Kamenetskii theory [3], for a low Mach number planar flame its propagation velocity relative to the gas is proportional to the square root of the reaction rate. On the other hand, the effective velocity of the wrinkled flame is proportional to its degree of folding Σ . Hence, the effective reaction rate of the wrinkled flame should be proportional to Σ^2 . Indeed, simulations of the Σ^2 – based model corroborate this assessment for moderately high Σ -s (see [4], [1] and Fig. 5 below). For general Mach numbers Σ^2 -model is clearly an extrapolation, hopefully providing a reasonably good description of the physics involved.

The following identities are used to close the above equation system.

- Components of shear stress tensors:

$$\begin{cases} \tau_{rr} &= -\frac{4}{3}\mu \left(\frac{\partial u}{\partial r} - \frac{u}{r} \right), \\ \tau_{\theta\theta} &= \frac{2}{3}\mu \left(\frac{\partial u}{\partial r} - \frac{u}{r} \right), \\ \tau_{\varphi\varphi} &= \frac{2}{3}\mu \left(\frac{\partial u}{\partial r} - \frac{u}{r} \right). \end{cases} \quad (4)$$

- Density

$$\rho = \sum_{i=1}^{n_s} W_i c_i \quad (5)$$

- Total specific energy:

$$\rho e = \sum_{i=1}^{n_s} c_i \left(h_i + \frac{1}{2} u^2 W_i \right) - P, \quad (6)$$

where h_i is the molar enthalpy and W_i is the molar mass of species i .

- Equation of state for ideal gas:

$$P = R^0 T \sum_{i=1}^{n_s} c_i, \quad (7)$$

where R^0 is the universal gas constant.

Here W_i denotes the molar mass of species i .

Coefficients of dynamic viscosity μ , heat conductivity λ and molar diffusion flux j_i^d are computed according to the mixture averaged formulation [5]:

- Dynamic viscosity of gas mixture

$$\mu = \sum_i \frac{X_i \mu_i}{\sum_j X_j \Phi_{ij}}, \quad (8)$$

- Heat conductivity

$$\lambda = \sum_i \frac{X_i \lambda_i}{\sum_j X_j \Phi_{ij}}. \quad (9)$$

- Molar diffusion flux

$$j_i^d = - \sum_j D_{ij}^c \frac{\partial c_j}{\partial r} \quad (10)$$

- Diffusion coefficient for concentrations, with correction for mass conservation $\sum_i W_i j_i^d = 0$ (see e.g. [6])

$$D_{ij}^c = X_i \left[(\delta_{ij} - X_i - Y_i) D_i^* + \sum_k Y_k D_k^* X_k \right], \quad (11)$$

Here the dimensionless factor, used for calculation of viscosity and heat conductivity coefficient is

$$\Phi_{ij} = \frac{1}{\sqrt{8}} \left(1 + \frac{W_i}{W_j} \right)^{-1/2} \left[1 + \left(\frac{\mu_i}{\mu_j} \right)^{1/2} \left(\frac{W_j}{W_i} \right)^{1/4} \right] \quad (12)$$

and diffusion coefficient for molar fractions

$$D_i^* = \frac{1}{X_i} \frac{1 - Y_i}{\sum_{j \neq i} X_j / \mathcal{D}_{ij}} = \frac{W_i}{Y_i W} \frac{1 - Y_i}{\sum_{j \neq i} X_j / \mathcal{D}_{ij}}, \quad (13)$$

with $X_i = c_i / \sum_j c_j$ and $Y_i = W_i c_i / \rho$ denoting molar and mass fractions respectively. \mathcal{D}_{ij} denotes binary diffusion coefficient between species i and j .

Molar enthalpies h_i are computed using the thermodynamic data, coded in NASA polynomial format [7].

Please note that Eqs. (3),(5) imply the conventional continuity equation,

$$\frac{\partial}{\partial t} (r^2 \rho) + \frac{\partial}{\partial r} (r^2 u \rho) = 0. \quad (14)$$

Our previous studies were concerned with the existence of a critical folding factor, when the deflagration flame propagation cannot be sustained [1, 4], and the role of detailed chemical reaction under such conditions [8], which assumes an application of a constant flame folding ratio. However, according to seminal Gostintsev's experimental observation [9] the flame folding in spherical geometry depends strongly on the flame radius:

$$\Sigma = \frac{3A^{2/3} R_f^{1/3}}{2u_p}, \quad (15)$$

where u_p is planar flame speed in relation to burned gas for $\Sigma = 1$. The factor A depends on mixture composition and pressure. For reaction $2\text{H}_2 + \text{O}_2$ under pressure of 1 bar: $A = 2500 \text{ m}^{1/3}/\text{s}^{1/2}$ [9] and $u_p = 90.5 \text{ m/s}$ [1].

The Maas-Warnatz mechanism [10] containing 8 species and 38 elementary reactions is used.

3 Initial and boundary conditions

In this setup, a sufficiently large computational domain is chosen, so that the acoustic waves do not disturb the solution by the reflection from the opposite boundary. For the current case, the domain $35.1 \text{ mm} \leq r \leq 100 \text{ m}$ (see Eq. (16)) was chosen. This domain allows a simulation time of about 190 ms until acoustic disturbances reach the opposite side, taking into account the speed of sound in the fresh mixture of 540 m/s. The position of the left boundary $R_0 = 35.1 \text{ mm}$ is chosen so that the folding factor starts with $\Sigma = 1$, according to Eq. (15).

$$\begin{cases} u(t, R_0) = u(t, R_\infty) = 0, \\ \frac{\partial}{\partial r} T(t, R_0) = \frac{\partial}{\partial r} T(t, R_\infty) = 0, \\ \frac{\partial}{\partial r} c_i(t, R_0) = \frac{\partial}{\partial r} c_i(t, R_\infty) = 0, \quad \forall i = 1, \dots, n_s, \end{cases} \quad (16)$$

where $R_0 = 35.1 \text{ mm}$ and $R_\infty = 100 \text{ m}$.

The ignition is initiated with a hot spot, keeping the initial pressure constant in space.

$$\begin{cases} u_0 = 0, \\ T_0(r) = 300 \text{ K} + (1700 \text{ K}) e^{-((r-R_0)/l)^2}, \\ c_{0,i}(r) = X_{i,0} \frac{1 \text{ bar}}{R^0 T_0(r)}, \quad i = 1, \dots, n_s, \end{cases} \quad (17)$$

where hot spot width is $l = 0.12 \text{ mm}$, which provides a minimal energy deposition.

4 Numerical method

The solution is integrated with the Adaptive Pseudo Spectral Element Method (APSEM) suggested in [1, 11]. The main idea of the method is to apply the pseudo-spectral method within a particular computational cell with a dynamically adaptive mesh generation via a priori user specified error control and by employing matching procedure [12]. The computational domain is split up into a number of sub-domains while matching the solution \mathbf{u} and its first derivative, e.g. $\partial(\mathbf{u})/\partial x$, at the boundaries, i.e. $\mathbf{u} = (u, T, c_1, \dots, c_{n_s})$.

The numerical method can be summarised as follows. The solution domain $r \in [R_0, R_\infty]$ on the time interval $t \in [t_a, t_b]$, where $t_0 \leq t_a < t_b \leq t_\infty$, is split up into a number of sub-domains

$$R_0 < \dots < r_l < \dots < R_\infty, \quad l = 1, 2, \dots, (N_r - 1), \quad (18)$$

and within each domain l , $r \in [r_l, r_{l+1}]$, the solution is approximated with a weighted sum of M_l basis functions

$$\mathbf{u}^l(t, r) = \sum_{i=0}^{M_l-1} \hat{\mathbf{u}}_i^l \varphi_i(t, r). \quad (19)$$

where $\hat{\mathbf{u}}_i$ are corresponding time dependent spectral coefficients. The number of subdomains N_r and the approximation order M_l are determined simultaneously with the solution \mathbf{u} within iterations for a one time step. The size of the time step and spacial adaptation depend on user specified tolerances (ATOL, RTOL), so that the maximal error does not exceed the specified values.

4.1 Solution within single numerical domain

Firstly, a solution with a global numerical domain is presented. Although the main component of the proposed method is the pseudo spectral method [12], the developed framework allows to easily adapt other spectral methods like the Galerkin weighted residual method. In order to derive the numerical method, the conservation equations can be written in the following form, with corresponding boundary and initial conditions:

$$\begin{cases} \frac{\partial}{\partial t} [\mathbf{f}_t(t, r, \mathbf{u})] + \frac{\partial}{\partial r} [\mathbf{f}_r(t, r, \mathbf{u}, \mathbf{u}')] = \mathbf{q}(t, r, \mathbf{u}, \mathbf{u}'), & t \in [t_0, t_\infty], \quad r \in [R_0, R_\infty] \\ \frac{\partial}{\partial t} [\mathbf{f}_0(t, \mathbf{u})] = \mathbf{q}_0(t, r, \mathbf{u}, \mathbf{u}'), & t \in [t_0, t_\infty] \quad r = R_0 \\ \frac{\partial}{\partial t} [\mathbf{f}_\infty(t, \mathbf{u})] = \mathbf{q}_\infty(t, r, \mathbf{u}, \mathbf{u}'), & t \in [t_0, t_\infty], \quad r = R_\infty \\ \mathbf{u}(t_0, r) = \mathbf{u}_0(r), & r \in [R_0, R_\infty] \end{cases}, \quad (20)$$

where \mathbf{f}_t , \mathbf{f}_x , \mathbf{q} , \mathbf{f}_0 , \mathbf{q}_0 , \mathbf{f}_∞ , \mathbf{q}_∞ are given vector functions and \mathbf{u} is the solution vector, $\mathbf{u}' = \frac{\partial}{\partial r} \mathbf{u}$, i.e.

$$\mathbf{f}_t = r^2 \begin{pmatrix} \rho u \\ \rho e \\ c_i \end{pmatrix}, \quad (21)$$

$$\mathbf{f}_r = r^2 \begin{pmatrix} \rho u^2 + \tau_{rr} \\ u(\rho e + P + \tau_{rr}) + \sum_{i=1}^{n_s} h_i j_i^d - \lambda \frac{\partial T}{\partial r} \\ u c_i + j_i^d \end{pmatrix}, \quad (22)$$

$$\mathbf{q} = r^2 \begin{pmatrix} -\frac{\partial P}{\partial r} + \frac{1}{r} (\tau_{\theta\theta} + \tau_{\varphi\varphi}) \\ 0 \\ \Sigma^2 \dot{\omega}_i \end{pmatrix}, \quad (23)$$

$$\mathbf{f}_0 = \mathbf{f}_\infty = \mathbf{0}, \quad (24)$$

$$\mathbf{q}_0 = \mathbf{q}_\infty = \begin{pmatrix} u \\ \frac{\partial}{\partial r} T \\ \frac{\partial}{\partial r} c_i \end{pmatrix}. \quad (25)$$

The approximation of the solution \mathbf{u} on an interval $t \in [t_a, t_b]$ and $r \in [r_a, r_b]$ is being sought as a weighted sum of M_l basis functions, see Eq. (19). It is also required that \mathbf{u} is Lipschitz continuous on the interval $t \in [t_a, t_b]$ and $r \in [r_a, r_b]$. It is also required that vector functions \mathbf{f}_t , \mathbf{f}_r , \mathbf{q} are approximated with the same set of basis functions:

$$\mathbf{f}(t, r) = \sum_{i=0}^{M_l-1} \hat{\mathbf{f}}_i \varphi_i(t, r). \quad (26)$$

Note, for an arbitrary large M_l the approximation leads to the function itself [12].

Using a set of given collocation points (t_i, r_i) , the relation of $M_l = M_l^t M_l^r$ spectral coefficients and the solution approximation on $M_l^p = (M_l^t - 1)M_l^r$ collocation points reads as follows:

$$\left\{ \begin{array}{l} \sum_{j=0}^{M_l^r-1} \hat{\mathbf{f}}_{t,j} \varphi_j(t_0, r_i) = \mathbf{q}(t_0, r_i, \mathbf{u}_0(r_i), \mathbf{u}'_0(r_i)) - \frac{\partial}{\partial r} \mathbf{f}_x(t_0, r_i, \mathbf{u}_0(r_i), \mathbf{u}'_0(r_i)), \\ \quad i = 0, \dots, M_l^r - 1, \\ \sum_{j=0}^{M_l^r-1} \hat{\mathbf{f}}_{t,j} \varphi_j(t_i, r_i) = \mathbf{f}_t(t_i, r_i, \mathbf{u}(t_i, r_i), \mathbf{u}'(t_i, r_i)), \\ \quad i = k_t M_l^r + k_r, \forall k_t = 0, \dots, M_l^t - 2 \wedge k_r = 0, \dots, M_l^r - 1, \end{array} \right. \quad (27)$$

and

$$\left\{ \begin{array}{l} \sum_{j=0}^{M_l^r-1} \hat{\mathbf{f}}_{x,j} \varphi_j(t_0, r_i) = \frac{\partial}{\partial r} \mathbf{f}_x(t_0, r_i, \mathbf{u}_0(r_i), \mathbf{u}'_0(r_i)), \quad i = 0, \dots, M_l^r - 1. \\ \sum_{j=0}^{M_l^r-1} \hat{\mathbf{f}}_{x,j} \varphi_j(t_i, r_i) = \mathbf{f}_x(t_i, r_i, \mathbf{u}(t_i, r_i), \mathbf{u}'(t_i, r_i)), \\ \quad i = k_t M_l^r + k_r, \forall k_t = 0, \dots, M_l^t - 2 \wedge k_r = 0, \dots, M_l^r - 1, \end{array} \right. \quad (28)$$

Eqs. (26), (27) and (28) can be more conveniently written in matrix-vector form:

$$\tilde{\mathbf{f}}_t = \hat{\mathbf{f}}_t \Phi, \quad (29)$$

$$\hat{\mathbf{f}}_t P_t = \left(\tilde{\mathbf{q}}^0 - \frac{\partial}{\partial r} \tilde{\mathbf{f}}_x^0, \tilde{\mathbf{f}}_t \right), \quad (30)$$

and

$$\hat{\mathbf{f}}_x P_x = \left(\frac{\partial}{\partial r} \tilde{\mathbf{f}}_x^0, \tilde{\mathbf{f}}_x \right), \quad (31)$$

where $\tilde{\mathbf{f}}_t, \tilde{\mathbf{f}}_x, \tilde{\mathbf{q}}$ are the solution approximations on the specified M_l^p collocation points and $\tilde{\mathbf{f}}_t^0, \tilde{\mathbf{f}}_x^0, \tilde{\mathbf{q}}^0$ are initial values at collocation points for $t = t_a$, such that

$$\tilde{\mathbf{f}}_{t,i} = \mathbf{f}_t(t_i, r_i, \mathbf{u}(t_i, r_i), \mathbf{u}'(t_i, r_i)), \quad (32)$$

$$\tilde{\mathbf{f}}_{x,i} = \mathbf{f}_x(t_i, r_i, \mathbf{u}(t_i, r_i), \mathbf{u}'(t_i, r_i)), \quad (33)$$

$$\tilde{\mathbf{q}}_i = \mathbf{q}(t_i, r_i, \mathbf{u}(t_i, r_i), \mathbf{u}'(t_i, r_i)), \quad (34)$$

$$\tilde{\mathbf{f}}_{t,i}^0 = \mathbf{f}_t(t_i, r_i, \mathbf{u}_0(r_i), \mathbf{u}'_0(r_i)), \quad (35)$$

$$\tilde{\mathbf{f}}_{x,i}^0 = \mathbf{f}_x(t_i, r_i, \mathbf{u}_0(r_i), \mathbf{u}'_0(r_i)), \quad (36)$$

$$\tilde{\mathbf{q}}_i^0 = \mathbf{q}_0(t_i, r_i, \mathbf{u}_0(r_i), \mathbf{u}'_0(r_i)), \quad (37)$$

Then time and space derivatives can be computed from the collocation points as

$$\dot{\tilde{\mathbf{f}}}_t = \left(\tilde{\mathbf{q}}_0 - \frac{\partial}{\partial r} \tilde{\mathbf{f}}_x^0, \tilde{\mathbf{f}}_t \right) P_t^{-1} \dot{\Phi} = \left(\tilde{\mathbf{q}}_0 - \frac{\partial}{\partial r} \tilde{\mathbf{f}}_x^0, \tilde{\mathbf{f}}_t \right) \dot{\mathbf{H}}, \quad (38)$$

and

$$\tilde{\mathbf{f}}'_x = \left(\frac{\partial}{\partial r} \tilde{\mathbf{f}}_x^0, \tilde{\mathbf{f}}_x \right) P_x^{-1} \Phi' = \left(\frac{\partial}{\partial r} \tilde{\mathbf{f}}_x^0, \tilde{\mathbf{f}}_x \right) \mathbf{H}'. \quad (39)$$

Similarly, the first derivative of a one dimensional time function $\mathbf{f}_t = \sum_i \hat{\mathbf{f}}_t \varphi_i(t)$ is $\dot{\mathbf{f}}_t = \left(\frac{d}{dt} \tilde{\mathbf{f}}_t^0, \tilde{\mathbf{f}}_t \right) G'_t$.

Using a set of test functions ψ_i a weak formulation can be written

$$\int_{t_a}^{t_b} \int_{r_a}^{r_b} \left[\frac{\partial}{\partial t} (\mathbf{f}_t) + \frac{\partial}{\partial r} (\mathbf{f}_r) \right] \psi_i dt dr = \int_{t_a}^{t_b} \int_{r_a}^{r_b} \mathbf{q} \psi_i dt dr, \forall i = 0, \dots, M_l^p - 1. \quad (40)$$

Introducing eq. (26) in eq. (40) and choosing test functions from the space of Dirac-delta functions $\psi_i(t, r) = \delta(t - t_i)\delta(r - r_i)$ one obtains a discrete form of conservation equations:

$$\left\{ \begin{array}{l} \sum_{j=M_l^r}^{M_l^p-1} \left(\tilde{\mathbf{q}}_j - \tilde{\mathbf{f}}_{t,j} \dot{h}_{j+M_l^r,i} - \tilde{\mathbf{f}}_{x,j} h'_{j+M_l^r,i} \right) \\ = \sum_{j=0}^{M_l^r-1} \left(\left(\tilde{\mathbf{q}}_j^0 - \frac{\partial}{\partial r} \tilde{\mathbf{f}}_{x,j}^0 \right) \dot{h}_{j,i} + \tilde{\mathbf{f}}_{t,j}^0 \dot{h}_{j+M_l^r,i} + \frac{\partial}{\partial r} \tilde{\mathbf{f}}_{x,j}^0 h'_{j,i} + \tilde{\mathbf{f}}_{x,j}^0 h'_{j+M_l^r,i} \right), \\ i = k_t M_l^r + k_r, \forall k_t = 1, \dots, M_l^t - 2 \wedge k_r = 1, \dots, M_l^r - 1, \\ \sum_{j=1}^{M_l^t-2} \left(\tilde{\mathbf{q}}_{0,j} - \tilde{\mathbf{f}}_{0,j} g_{j+1,i}^t \right) = \tilde{\mathbf{q}}_{0,0}^0 g_{0,0}^t + \tilde{\mathbf{f}}_{0,0}^0 g_{1,0}^t, \quad \forall i = 1, \dots, M_l^t - 2, \\ \sum_{j=1}^{M_l^t-2} \left(\tilde{\mathbf{q}}_{\infty,j} - \tilde{\mathbf{f}}_{\infty,j} g_{j+1,i}^t \right) = \tilde{\mathbf{q}}_{\infty,0}^0 g_{0,0}^t + \tilde{\mathbf{f}}_{\infty,0}^0 g_{1,0}^t, \quad \forall i = 1, \dots, M_l^t - 2. \end{array} \right. \quad (41)$$

If the number of basis function in time direction is $M_l^t = 3$, the time marching scheme is equivalent to the well known trapezoidal (Crank-Nicolson) method (see e.g. [13]), which is $O(2)$ accurate. In the current study we use: for space – Chebyshev polynomials of the first kind of variable order ($M_l^r \leq 16$) with Gauss-Lobatto collocation points [12], and for time – power series of the second order ($M_l^t = 3$) with equidistant points, i.e. for time interval $t \in [t_a, t_b]$ and space – $r \in [r_l, r_{l+1}]$ it reads as

$$\varphi_i(t, r) = \varphi_j^t(t) \varphi_k^r(r) = \left(\frac{t - t_a}{t_b - t_a} \right)^j T_k \left(2 \frac{r - r_l}{r_{l+1} - r_l} - 1 \right), \quad (42)$$

where $i = jM_l^r + k$, T_k is k -th Chebyshev polynomial of the first kind and $M_l = M_l^t M_l^r$ with M_l^t is the number of basis functions in time direction and M_l^r is the number of basis functions in space direction. Note, however, the presented algorithm can be used with other types of basis functions. For an elaborated description of the method the reader is referred to [11].

The system (41) is a non-linear algebraic equation, which is solved implicitly with Newton's method (see e.g. [13]).

4.2 Domain matching and boundary conditions

The solution in time is being sought one time-interval after the other: the initial condition $\mathbf{u}(t_k)$ on the interval $t \in [t_k, t_{k+1}]$ is provided from the solution of the previous interval $t \in [t_{k-1}, t_k]$.

The subdomains in space are matched with the following boundary conditions:

$$\left\{ \begin{array}{l} \mathbf{u}_l(t, r_{l-1}) = \mathbf{u}_{l-1}(t, r_{l-1}) \\ \mathbf{u}_l(t, r_l) = \mathbf{u}_{l+1}(t, r_l) \\ \frac{\partial}{\partial x} \mathbf{u}_l(t, r_{l-1}) = \frac{\partial}{\partial r} \mathbf{u}_{l-1}(t, r_{l-1}) \\ \frac{\partial}{\partial x} \mathbf{u}_l(t, r_l) = \frac{\partial}{\partial r} \mathbf{u}_{l+1}(t, r_l), \end{array} \right. \quad (43)$$

where \mathbf{u}_l is solution approximation within domain l . Note, first and last collocation points (Gauss-Lobatto) are placed exactly at the boundary. The evolution of these points (*knots*) is governed by eqs. (43), whilst points within a space interval (*cell*) are governed by PDE eqs. (20).

4.3 Grid adaptation

In order to introduce the grid adaptation strategy, the error control strategy is first presented. The absolute interpolation error of the state variable u_i for the number of basis functions M is limited by the factor of 2 of the series last coefficient [12], but even in converging series, under particular conditions, some coefficients can be naturally zeros, whilst others are non-zero. For these reasons the following approximation of the absolute error of variable u_i has been suggested and used:

$$e_i^{\text{abs}} = \sqrt{\hat{u}_{i,M}^2 + \hat{u}_{i,M-1}^2}, \quad \forall i = 0, \dots, n_v - 1, \quad (44)$$

where $\hat{u}_{i,k}$ is the amplitude of the k -th coefficient of the series expansion. The last equation is used in order to deal with spurious zeros of spectral coefficients. Then the normalized relative error is defined as:

$$E = \max_{i=1, \dots, n_v} \frac{e_i^{\text{abs}}}{\text{RTOL}_i (\text{ATOL}_i + |\hat{u}_{i,0}|)}. \quad (45)$$

When eq. (45) is applied for each time slice, corresponding to time collocation points, the measure of space error E^r is derived. When the equation is applied for each space slice, corresponding to space collocation points, the measure of time error E^t is computed.

The time adaptation is reflected in the size of time interval, while keeping the order of polynomial along time direction constant, e.g. $M_l^t = 3$. The procedure of the time step adaptation is covered by standard numerical recipes (see e.g. [13]).

The adaptation strategy in space direction r consists of two parts: one is to adjust the polynomial order within one computational cell; the other is to split/join cells. The first strategy becomes rapidly computationally expensive for large polynomial orders, e.g. for $M_l^r > 16$, due to the computationally expensive inversion of large dense matrices. However, the error of approximation is sinking exponentially with the polynomial order. The cell splitting creates more collocation points and is hampered by memory reallocation, compared to the polynomial order increase, but it is outweighed by a faster global solution of the linear system and allows to avoid spectral blocking when the relatively stiff behaviour of the solution takes place.

If the accuracy within a cell l is insufficient, i.e. $E_l^r > 1$, the adaptation consists of two stages:

1. Increase polynomial order within cell till it reaches $M_l^r = 16$, if the error is still above unity;
2. Split computational cell.

If the accuracy within the cell l exceeds requirements (specified tolerances), i.e. $E_l^r < 0.01$, the adaptation consist again of two stages:

1. Decrease polynomial order within the cell until it reaches $M_l^r = 4$, if the the error is still below unity;
2. If the adjacent cell has also reached the minimal polynomial order, merge both cells to one cell, while keeping the order $M_l^r = 4$.

The specified maximal order $M_l^r = 16$, minimal order $M_l^r = 4$, minimal normalised error $E_l^r = 0.01$ are customisable parameters, which to a large extent depend on a type of polynomial approximation. By the reduction of polynomial order and by joining of computational cells it is important to enforce not only boundary values (imposed automatically) but also gradients at the boundary (see Eq. 43).

5 Results and discussions

Fig. 1 shows pressure (left) and temperature (right) profiles, plotted every $0.5 \mu s$, as well as the state at the DDT point. Fig. 2 shows the corresponding density and velocity profiles. The observed transition radius and critical flame folding ratio are $R_{ddt} = 9.965 \text{ m}$ and $\Sigma_{ddt} = 6.57$. In our previous work [1] we estimated in planar symmetry the transition radius $R_{ddt}^* = 8.377$ and the corresponding critical flame folding ratio $\Sigma_{ddt}^* = 6.25$. The latter values as expected are slightly less than in the current spherical case.

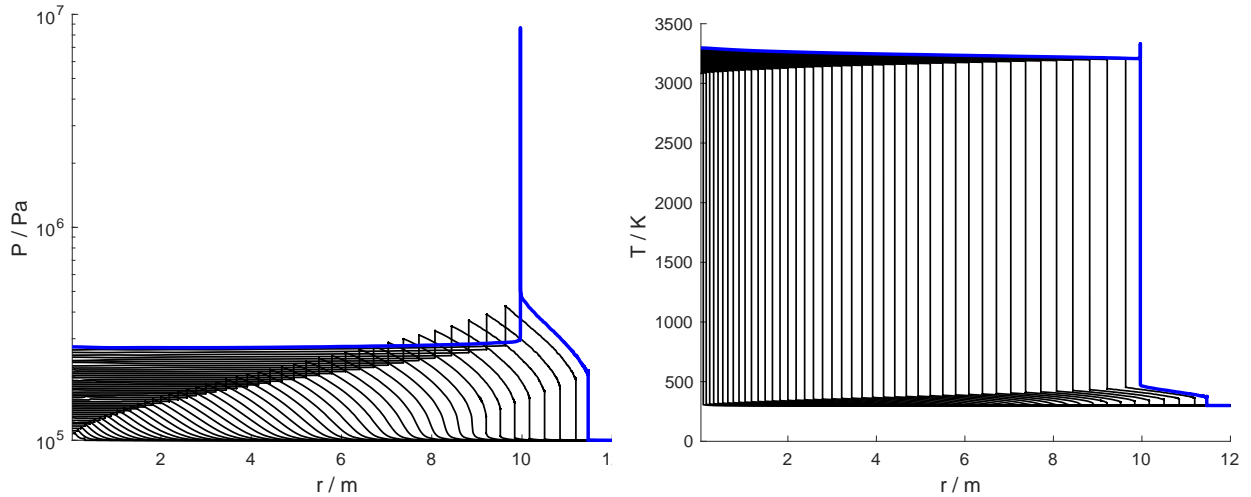


Figure 1: Pressure (left) and temperature (right) profiles every $0.5 \mu s$. Blue line corresponds to DDT.

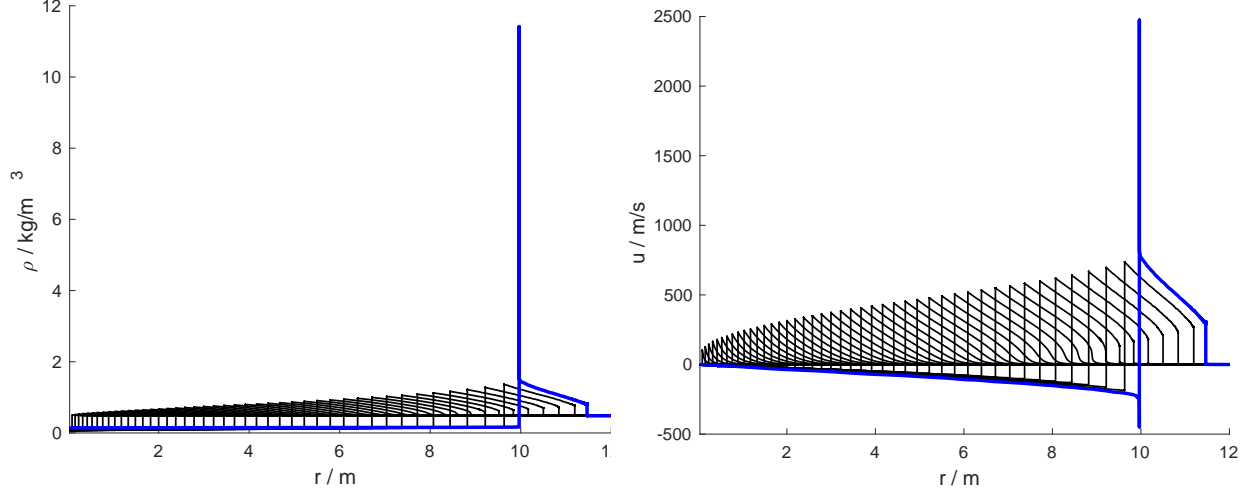


Figure 2: Density (left) and flow velocity (right) profiles every $0.5 \mu s$. Blue line corresponds to DDT.

Although a smooth ignition was applied (providing ignition energy less by 1 % leads to ignition failure), a generated during the ignition shock wave is traveling ahead of the flame. This is shown on the pressure zoomed pressure profile Fig. 3.

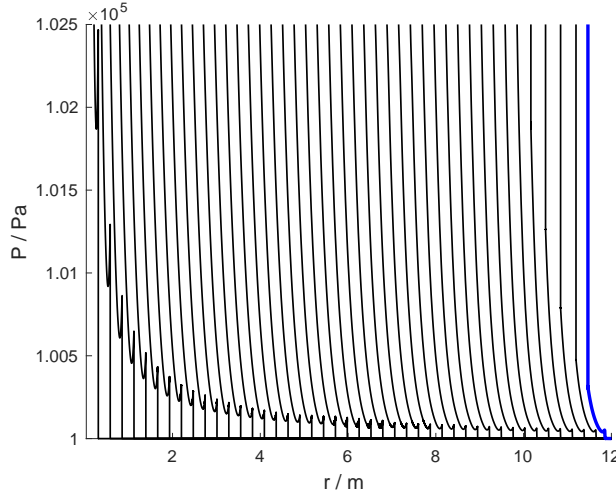


Figure 3: Zoomed pressure profiles for every $0.5 \mu s$. Blue line corresponds to DDT.

Positions of flame front R_f and of the precursor shock R_s at different time instances are shown in Fig. 4 (left). Correspondingly the flame front velocity D_f and the velocity of the precursor shock D_s are shown in Fig. 4 (right). As one may expect, the speed of the precursor shock is close to the speed of sound a_0 in the unburned mixture, which is plotted by the green line. Note that these green and blue lines practically coincide. In order to compute the speed of sound the following expression is used [14]:

$$a = \sqrt{\gamma \frac{P}{\rho}}, \quad (46)$$

where

$$\gamma = \frac{\sum_i c_i C_{p_i}}{\sum_i c_i (C_{p_i} - R^0)} \quad (47)$$

is the adiabatic index for an ideal gas and C_{p_i} is the molar heat capacity at constant pressure.

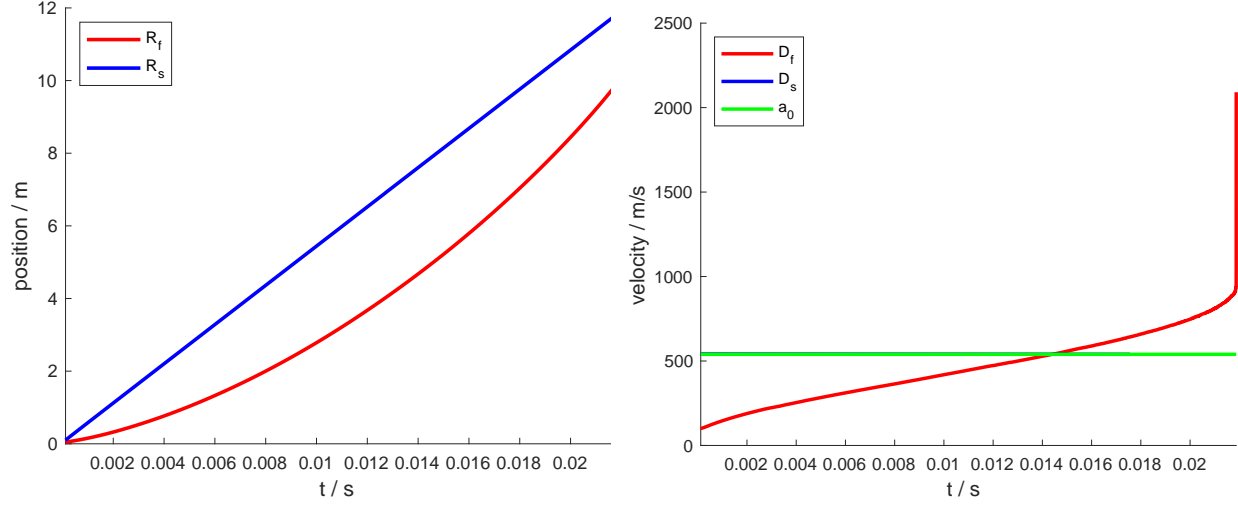


Figure 4: Flame and shock position vs. time (left); flame flame and shock velocity vs. time (right).

As is readily seen the flame speed D_f increases and may even exceed a_0 . Yet, approaching the DDT point the accelerating flame stays behind the precursor shock: $R_{ddt} = 10$ m while $R_{s,ddt} = 11.5$ m. In Fig. 5 $u_0 = u(R_f + 5 \text{ mm})$, $u_b = u(R_f - 5 \text{ mm})$ corresponding respectively to the approximate entry/exit into/from the reaction zone. Since $D_f - u_b < a_b$, the pre-DDT flame does not reach the threshold of CJ-deflagration. Approaching the transition point Σ -dependency of $D_f - u_b$ becomes nonlinear. This can be attributed to the elevated pressure and temperature in the compressed region between R_f and R_s , conducive to a higher burning velocity.

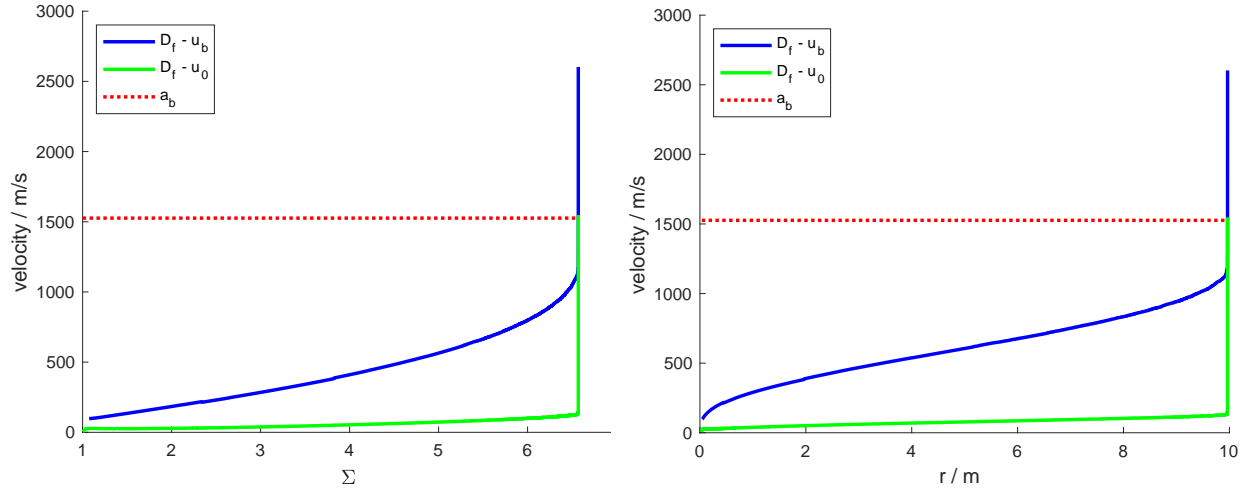


Figure 5: Flame front velocity relative to the entry (green) and to the exit (blue) from the reaction zone, as a function of folding ratio (left) and as a function of flame position (right).

Acknowledgement

These studies were supported by the US-Israel Binational Science Foundation (Grant 2012-057) and the Israel Science Foundation (Grant 335/13).

References

- [1] A. Koksharov, V. Bykov, L. Kagan, G. Sivashinsky, Deflagration-to-detonation transition in an unconfined space, *Combustion and Flame* 195 (2018) 163–169.
- [2] B. Deshaies, G. Joulin, Flame-speed sensitivity to temperature changes and the deflagration-to-detonation transition, *Combustion and flame* 77 (2) (1989) 201–212.
- [3] Y. B. Zeldovich, G. I. Barenblatt, V. B. Librovich, G. Makhviladze, *Mathematical theory of combustion and explosions*, Springer, New York, 1985.
- [4] L. Kagan, G. Sivashinsky, Parametric transition from deflagration to detonation: Runaway of fast flames, *Proceedings of the Combustion Institute* 36 (2) (2017) 2709–2715.
- [5] R. B. Bird, W. E. Stewart, E. N. Lightfoot, *Transport phenomena*, revised 2. ed. Edition, Wiley, New York, 2007.
- [6] R. J. Kee, M. E. Coltrin, P. Glarborg, *Chemically reacting flow: theory and practice*, Wiley Interscience, Hoboken, NJ, 2003.
- [7] R. A. Svehla, Estimated viscosities and thermal conductivities of gases at high temperatures, Technical report, NASA, Washington, 1962.
- [8] V. Bykov, A. Koksharov, Study of internal flame front structure of accelerating hydrogen/oxygen flames with detailed chemical kinetics and diffusion models, *Math. Model. Nat. Phenom.* 13 (6).
- [9] Y. A. Gostintsev, A. G. Istratov, Y. V. Shulenin, Self-similar propagation of a free turbulent flame in mixed gas mixtures, *Combustion, Explosion and Shock Waves* 24 (5) (1988) 563–569.
- [10] U. Maas, J. Warnatz, Ignition processes in hydrogen-oxygen mixtures, *Combustion and Flame* 74 (1) (1988) 53–69.
- [11] V. Bykov, A. Kiverin, A. Koksharov, I. Yakovenko, Analysis of transient combustion with the use of contemporary cfd techniques, *Computers and Fluids*, submitted.
- [12] J. P. Boyd, *Chebyshev & Fourier spectral methods*, Lecture notes in engineering, Springer, Berlin, 1989.
- [13] A. Quarteroni, R. Sacco, F. Saleri, *Numerical mathematics*, Texts in applied mathematics, Springer, New York, 2000.
- [14] F. A. Williams, *Combustion theory: the fundamental theory of chemically reacting flow systems*, 2nd Edition, Combustion science and engineering series, Addison Wesley, Redwood City, Calif., 1988.